Available online at www.sciencedirect.com
ScienceDirect
Journal of Nuclear Materials 376 (2008) 11–28
journal of nuclear materials
www.elsevier.com/locate/jnucmat

Low temperature neutron irradiation effects on microstructure and tensile properties of molybdenum

Meimei Li [a,], M. Eldrup [b], T.S. Byun [a], N. Hashimoto [c], L.L. Snead [a], S.J. Zinkle [a]

[a] *Materials Science and Technology Division, Oak Ridge National Laboratory, Oak Ridge, TN 37831, USA*
[b] *Materials Research Department, Risø National Laboratory, Technical University of Denmark, DK-4000, Roskilde, Denmark*
[c] *Materials Science Division, Hokkaido University, Sapporo 060-8628, Japan*

Received 5 June 2007; accepted 12 December 2007

Abstract

Polycrystalline molybdenum was irradiated in the hydraulic tube facility at the High Flux Isotope Reactor to doses ranging from 7.2×10^{-5} to 0.28 dpa at ~80 °C. As-irradiated microstructure was characterized by room-temperature electrical resistivity measurements, transmission electron microscopy (TEM) and positron annihilation spectroscopy (PAS). Tensile tests were carried out between −50 and 100 °C over the strain rate range 1×10^{-5} to 1×10^{-2} s^{-1}. Fractography was performed by scanning electron microscopy (SEM), and the deformation microstructure was examined by TEM after tensile testing. Irradiation-induced defects became visible by TEM at ~0.001 dpa. Both their density and mean size increased with increasing dose. Submicroscopic three-dimensional cavities were detected by PAS even at ~0.0001 dpa. The cavity density increased with increasing dose, while their mean size and size distribution was relatively insensitive to neutron dose. It is suggested that the formation of visible dislocation loops was predominantly a nucleation and growth process, while in-cascade vacancy clustering may be significant in Mo. Neutron irradiation reduced the temperature and strain rate dependence of the yield stress, leading to radiation softening in Mo at lower doses. Irradiation had practically no influence on the magnitude and the temperature and strain rate dependence of the plastic instability stress.

1. Introduction

Molybdenum is of great interest for high temperature applications in advanced fission and fusion reactor systems because of its high melting point, excellent high temperature strength, good thermal conductivity, resistance to irradiation-induced swelling and corrosion resistance in liquid metal coolants [1]. However, Mo, like other body-centered cubic (bcc) metals, is susceptible to low temperatures embrittlement and suffers an increase in ductile-brittle transition temperature (DBTT) after neutron exposure [2–11]. The improvement in low temperature ductility of neutron-irradiated Mo is of great importance for its applications in advanced nuclear systems.

Low temperature embrittlement is associated with irradiation hardening that is controlled by the interactions of mobile dislocations and irradiation-induced defects. Whether or not Mo can be engineered to resist irradiation-induced low temperature embrittlement is dependent on the formation process of sessile defect clusters in Mo. It is known that two formation processes are often competing during irradiation, namely in-cascade clustering and diffusive nucleation and growth. If the formation of sessile defect clusters is dominated by a nucleation and growth process such as in bcc Fe [12–16], solute additions may have a strong effect on the formation of defect clusters and radiation hardening. The resistance to irradiation embrittlement may, therefore, be improved by metallurgical approaches. On the other hand, if large, sessile defect clusters originate from displacement cascades, e.g. in bcc W [12–14,17], the low temperature irradiation embrittlement is essentially an inherent problem, and may not be overcome.

Corresponding author. Present address: Argonne National Laboratory. Tel.: + 1 630 2525111; fax: + 1 630 2523604.
E-mail address: mli@anl.gov (M. Li).

0022-3115/$ - see front matter © 2008 Published by Elsevier B.V.
doi:10.1016/j.jnucmat.2007.12.001

Defect formation and accumulation in irradiated materials is influenced largely by crystalline structure and atomic mass. Molecular dynamic (MD) simulations and heavy-ion irradiation experiments have clearly showed that displacement cascades are more compact and production efficiency of visible defect clusters is greater in fcc Cu than in bcc Fe [12,13,18–21]. The difference is primarily due to the more compact lattice structure of fcc metals vs. the more open lattice structure of bcc metals. The mass difference between metals is important in the defect production and accumulation as well. The displacement cascades were found to be more compact, and the energy threshold for subcascade formation is higher in a high-mass metal than in a medium-mass metals, such as bcc Mo vs. bcc Fe [20,21]. These differences in displacement cascades have significant implications in in-cascade clustering and defect cluster evolution.

While the fundamentals of defect production and evolution in medium-mass metals, such as fcc Cu, Ni and bcc Fe are well established, the understanding of defect production in high-mass metals such as fcc Pd and bcc Mo and W is still limited. Recent MD computer simulations of atomic displacement cascades in Mo [20] have provided new insights into the primary radiation damage in Mo, and have identified the differences in in-cascade clustering behavior between medium-mass bcc Fe and high-mass bcc Mo. Validation of these simulation results requires experimental evidence from well-designed mechanistic neutron irradiation experiments such as low temperature, low dose neutron irradiation. One of the primary interests of this study is to provide direct measurements of defect clusters and resultant hardening to validate in-cascade clustering results obtained from MD simulations.

The interaction between irradiation-induced defect clusters and glide dislocations is the key to understand the hardening and embrittlement in irradiated Mo. Irradiation hardening not only depends on the nature and size of defect clusters effective as barriers to dislocation motions, but also can be strongly affected by the strain rate and test temperature [22–30]. In contrast to fcc crystals, a large temperature and strain rate dependence of yielding occurs in bcc metals even in unirradiated conditions. The yield stress increases rapidly with decreasing temperature and increasing strain rate in unirradiated Mo [31]. A good understanding of the radiation hardening mechanism in bcc Mo requires detailed studies of neutron irradiation effects on the temperature and strain rate dependence of the flow stress. Temperature and strain rate-insensitive irradiation hardening implies that irradiation does not affect the rate-controlling deformation mechanism operative in the unirradiated condition, i.e. athermal hardening resulted from long-range barriers, while temperature and strain rate-sensitive irradiation hardening indicates that irradiation-induced obstacles can be overcome by dislocations with thermal assistance, i.e. thermal hardening from short-range barriers [23]. The study on the dependence of the true stress at the ultimate tensile strength, so-called plastic instability stress (PIS) on the temperature and the strain rate is lacking.

The increase in yield stress is often accompanied by a loss of strain hardening capacity and tensile ductility, and can also lead to embrittlement by shifting the DBTT to a higher temperature. Plastic deformation tends to occur in an inhomogeneous manner and to be localized in dislocation channels after irradiation. Premature plastic instability occurs at yield once the yield strength reaches the level of the PIS of an irradiated material [32–35]. Wechsler [36] suggested that the low temperature irradiation embrittlement is likely associated with changes in plastic properties, particularly with inhomogeneous plastic deformation rather than changes in inherent fracture processes. Crack formation from coarse slip steps and the intersection of coarse slip bands was suggested to cause 'channel fracture' [37,38]. Cracks may also initiate at grain boundaries due to local stress concentration caused by dislocation pile-up in a defect-free channel [5]. Direct correlation between dislocation channeling and premature plastic instability and correlation between dislocation channeling and radiation embrittlement, however, have not been confirmed by experiments.

The experiments described in this paper were designed to understand the role of in-cascade clustering in the formation of sessile defect clusters and the nature of interactions between irradiation-induced defects and moving dislocations. The ultimate purpose is to determine whether or not the resistance to low temperature embrittlement of irradiated Mo can be improved by metallurgical approaches. Neutron irradiation experiments were performed at seven low doses over a range of 7.2×10^{-5} to 0.28 dpa at reactor ambient temperature (~80 °C) on pure Mo. The formation of sessile defect clusters was investigated by characterizing as-irradiated microstructure by electrical resistivity, transmission electron microscopy (TEM), and positron annihilation spectroscopy (PAS). Irradiation hardening mechanisms in Mo were understood by examining the dose, temperature and strain rate dependence of the yield stress from tensile properties measurements between −50 and 100 °C at strain rates over the range of 1×10^{-5} to $1 \times 10^{-2}\,s^{-1}$. Deformation microstructure of irradiated specimens was examined after tensile testing. Fracture surfaces of broken tensile specimens were observed by scanning electron microscopy (SEM). The effects of neutron irradiation on strain hardening, plastic instability and fracture in Mo was described, and deformation and fracture mechanisms in neutron-irradiated Mo were discussed.

2. Experimental procedure

The material examined was low-carbon arc-cast (LCAC) Mo with purity >99.95% and interstitial impurity contents of 140 wppm C, 6 wppm O and 8 wppm N. Subsize SS-3 sheet tensile specimens with gauge dimensions of $7.62 \times 1.52 \times 0.50$ mm and rectangular coupon speci-

mens with dimensions of $25.4 \times 4.95 \times 0.25$ mm were machined from a cold-rolled 0.5 mm thick sheet. Coupon specimens were used for TEM microstructural characterization and PAS measurements. Following machining, specimens were annealed at 1200 °C for 1 h in high vacuum, resulting in an equiaxed grain structure with a grain size of 70 μm.

Irradiation of specimens was carried out in the hydraulic tube facility in the High Flux Isotope Reactor at the Oak Ridge National Laboratory. Specimens were loaded in perforated rabbit capsules allowing contact with the flowing coolant in the hydraulic tube to maintain the specimen temperature at ~80 °C. Specimens were irradiated to neutron fluences in the range of 2×10^{21} to 8×10^{24} n/m^2 ($E > 0.1$ MeV), corresponding to displacement damage levels 7.2×10^{-5}, 7.2×10^{-4}, 7.2×10^{-3}, 0.072 and 0.28 dpa. Unexpected weight loss and thickness reduction was observed on the specimens irradiated to high neutron fluences due to corrosion of molybdenum in coolant water. Two additional perforated rabbit capsules were irradiated to ensure water reaction had no effect on the results. In this additional irradiation experiment, tensile specimens were individually wrapped in thin high-purity Al foil and vacuum-sealed by electron-beam welding to minimize thermal gradients between the specimens and the flowing water. The thin-foil-wrapped specimens were then irradiated at ~80 °C to neutron fluences of 8.4×10^{22} n/m^2 and 8.1×10^{23} n/m^2 ($E > 0.1$ MeV), corresponding to displacement damage doses of 0.003 and 0.029 dpa. Post-irradiation measurements of electrical resistivity, as-irradiated microstructure and tensile properties showed consistent results with data obtained in the first experiment.

As-irradiated microstructure was examined by TEM to characterize defect cluster density, mean size and size distribution. The 3 mm discs were punched from coupon specimens or the grip regions of tensile specimens. Disc specimens were electropolished in a Tenupol twin-jet polishing unit using a solution of 7:1 methanol and sulphuric acid cooled to −10 °C. Microstructure examination was performed using combined bright field (BF) and weak beam dark field (WBDF) imaging techniques. Weak beam dark field imaging conditions were at ($g/5g$ or $g/6g$, $g = 110$) near a zone axis of $[\bar{1}\,1\,1]$. The defect cluster density and size measurements were made from WBDF images. The defect density measurements were checked by plotting the areal density vs. foil thickness, and the volumetric density was determined by the slope of the plot [15].

Positron annihilation spectroscopy measurements were conducted on 5×5 mm specimens cut from coupon specimens for each neutron dose. The specimens were electropolished before the measurements to remove surface effects. A conventional positron lifetime spectrometer was used in the measurements, and the details of the technique are given in Refs. [39,40]. All specimens were measured several times to assure reproducibility. The results for each dose are based on lifetime spectra that typically contain a total of 12–16×10^6 counts. The recorded spectra were evaluated using the PALSfit program [41].

Table 1
Tensile test conditions

Dose (dpa)	Test Temperature (°C)	Strain rate (s^{-1})	Dose (dpa)	Test Temperature (°C)	Strain rate (s^{-1})
Unirr.	−100	1×10^{-3}	Unirr.	22	1×10^{-1}
	−50	1×10^{-3}		22	1×10^{-2}
	−25	1×10^{-3}		22	1×10^{-3}
	22	1×10^{-3}		22	1×10^{-4}
	100	1×10^{-3}		22	1×10^{-5}
7.2×10^{-5}	−50	1×10^{-3}	0.003	22	1×10^{-2}
	−25	1×10^{-3}		22	1×10^{-3}
	22	1×10^{-3}		22	1×10^{-4}
	100	1×10^{-3}		22	1×10^{-5}
7.2×10^{-4}	−50	1×10^{-3}	0.029	22	1×10^{-3}
	22	1×10^{-3}		22	1×10^{-4}
	100	1×10^{-3}		22	1×10^{-5}
0.0072	−50	1×10^{-3}			
	−25	1×10^{-3}			
	22	1×10^{-3}			
	100	1×10^{-3}			
0.072	−50	1×10^{-3}			
	−25	1×10^{-3}			
	22	1×10^{-3}			
	100	1×10^{-3}			
0.28	22	1×10^{-3}			
	100	1×10^{-3}			

Electrical resistivity was measured on tensile specimens at room temperature before and after irradiation using a four-point probe technique following the guidelines in ASTM Standard Test Method for Resistivity of Electrical Conductor Materials ASTM B 193-02.

Tensile tests were conducted on unirradiated and irradiated specimens between −50 and 100 °C in air or a mixed

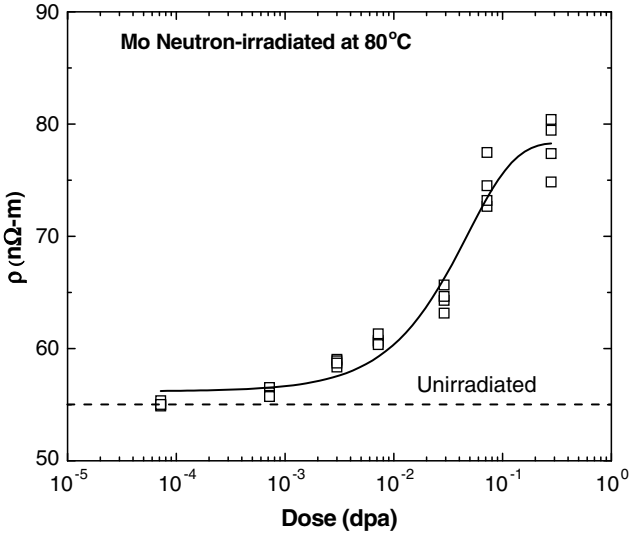

Fig. 1. Room-temperature electrical resistivity of neutron-irradiated Mo as a function of neutron dose. The mean value of electrical resistivity for unirradiated Mo is indicated by the dash line.

air and cold nitrogen environment at a strain rate over a range from 1×10^{-5} to 1×10^{-1} s^{-1}. The tensile test conditions are given in Table 1. Load and displacement data were recorded and used to determine stress–strain curves and tensile properties. Fractographic examinations were performed by SEM after tensile testing. The SEM images taken at low magnification (30×–50×) were used to determine final areas of the cross-section, and the reduction in

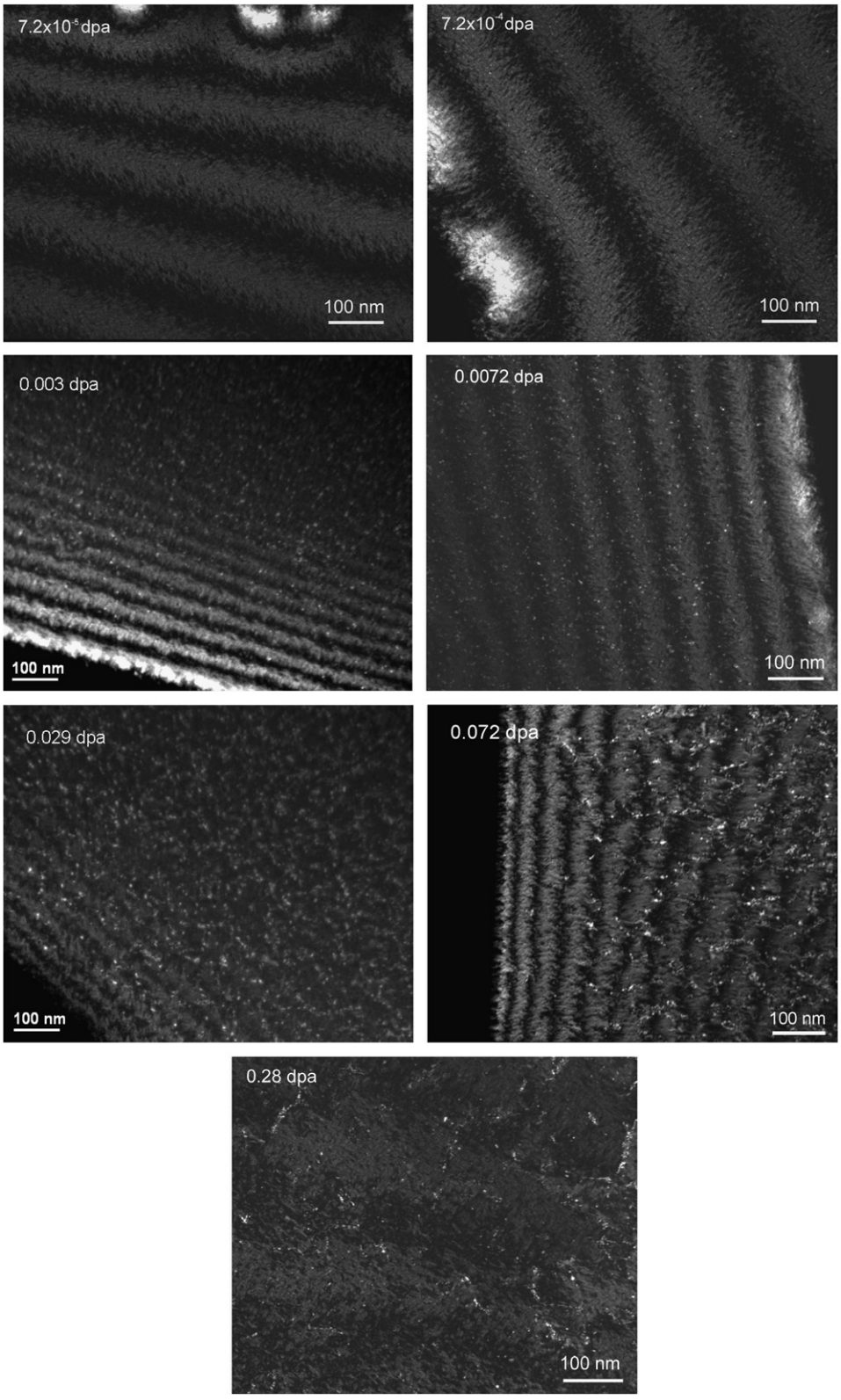

Fig. 2. Weak beam dark field images of defect clusters at different dose levels taken with a $[\bar{1}\,1\,1]$ zone axis and $g = [1\,1\,0]$ ($g/5g$, $6g$). Rafts (aligned groups of dislocation loops in a row) were observed at higher doses.

area (RA) was calculated as the percent change in cross-sectional area at failure.

The deformed microstructure of irradiated specimens was examined by TEM in the uniformly strained gauge section of broken tensile specimens.

3. Results

3.1. As-irradiated microstructure

3.1.1. Room-temperature electrical resistivity

The dose dependence of room-temperature electrical resistivity for neutron-irradiated Mo is shown in Fig. 1. The data points for each dose are the mean values of five measurements from four unique specimens. The mean value of electrical resistivity for unirradiated Mo is indicated by the dash line. No measurable change in electrical resistivity was observed after irradiation to the lowest dose, 7.2×10^{-5} dpa. An initial low rate of resistivity increase was followed by a high rate between ~0.01 and 0.1 dpa, followed by an asymptotic approach to a saturation value at doses above 0.1 dpa. Calculations showed that the influence of the neutron-induced transmutation products on resistivity change in the irradiated specimens was insignificant. Detailed discussion is given elsewhere [42].

3.1.2. Microstructure characterization by TEM

Fig. 2 shows representative WBDF images for Mo irradiated in the dose range from 7.2×10^{-5} to 0.28 dpa. The defect cluster density and mean size are plotted as a function of dose in Fig. 3, and the size distribution are plotted as the histograms with 0.5 nm intervals in Fig. 4. Fig. 3 also includes published data on pure Mo and Mo alloys that were neutron-irradiated at 50–100 °C for comparison [9–11,43,44]. As shown in Fig. 2, the as-irradiated microstructure consisted of uniformly-distributed dislocation loops at lower doses. The nature of the loops could not be resolved due to their small sizes. Previous studies on Mo annealed following irradiation have found that the dislocation loops are predominantly interstitial-type and have the Burgers vectors $\mathbf{b} = a/2\langle 111\rangle$ [45–50]. A highly-aggregated loop structure, so-called rafts, was observed at higher doses. Raft formation was detectable in the 0.0072 dpa specimen, indicated by aligned groups of two or three dislocation loops in a row. The formation of rafts became more pronounced as dose increased, and the raft length increased significantly with increasing dose.

A strong dose dependence of defect cluster density was observed in Mo. No visible defect clusters were observed in the 7.2×10^{-5} dpa specimen. The visible cluster density initially increased with increasing dose, reached a maximum at 0.029 dpa, and then decreased with increasing dose. The mean cluster size was dependent on irradiation dose as well. The mean cluster size increased linearly with dose from 1.94 to 3.36 nm between 7.2×10^{-4} and 0.28 dpa. The cluster size distribution showed two characteristic features: a shift of peaks to the large cluster size and a longer tail at large cluster size with increasing doses.

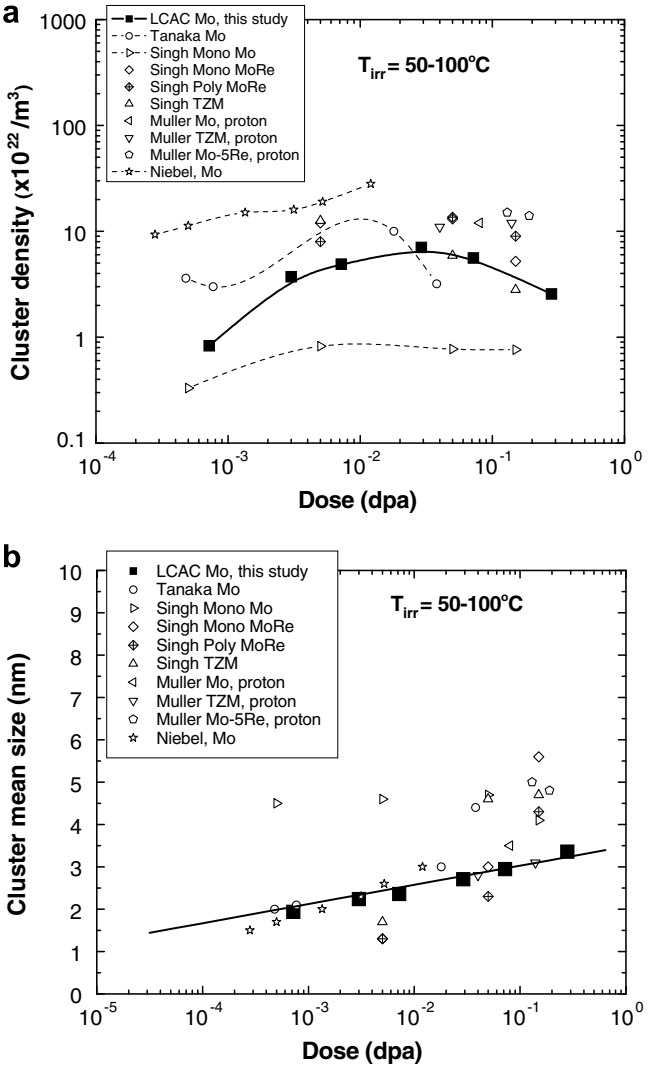

Fig. 3. Dose dependence of (a) defect cluster density and (b) defect cluster mean size in neutron-irradiated Mo (solid lines show the data of this study).

Weak contrast resembling cavities was revealed at high magnifications ($300k\times$) only in the 0.28 dpa specimen. Detailed characterization of cavities was difficult due to weak contrast. The estimated cavity density from TEM micrographs was on the order of 10^{23} m^{-3} with a mean size near the TEM resolution limit (~1 nm).

3.1.3. Microstructure characterization by PAS

Positron annihilation spectroscopy is particularly sensitive to the size and density of vacancy type defects, typically in the size range from mono-vacancies up to nano-voids containing ~50–100 vacancies and of densities of the order of parts per million. As discussed in some detail in the reference [51], it is possible to estimate size distributions of nanometer-sized cavities in irradiated materials. Based on such estimates, the total cavity density and the

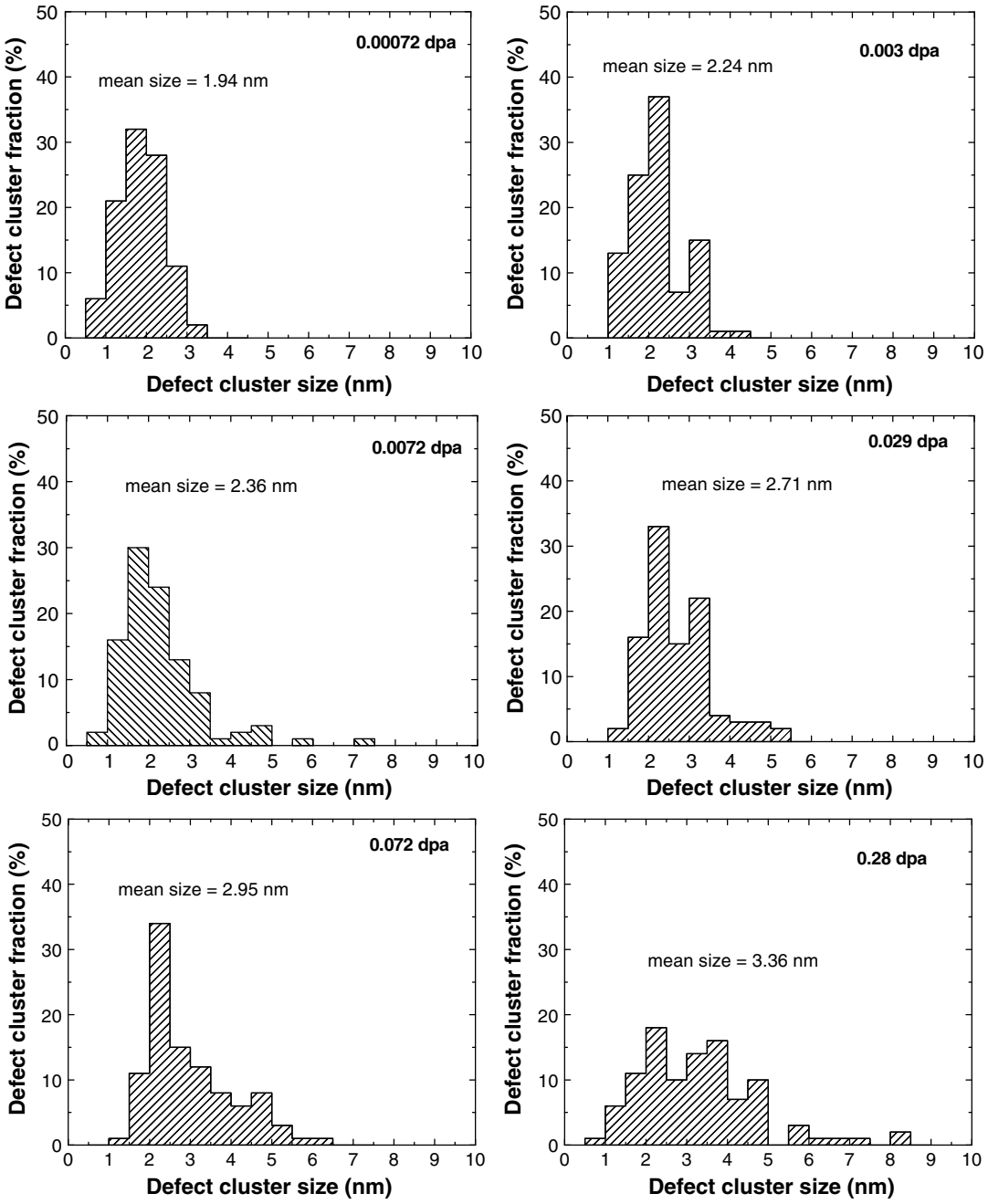

Fig. 4. The size distribution of TEM-visible defect clusters in neutron-irradiated Mo.

mean diameter can be calculated as a function of dose. The positron lifetime spectra for Mo were analyzed on the assumption that the distribution of lifetimes can be approximated by four bins: 190, 260, 350 and 470 ps, equivalent to three-dimensional vacancy clusters containing 1, 3, 10 and 50 or more vacancies, respectively. The calculated size distributions for the vacancy clusters are shown in Fig. 5(a), and the total cavity density and the mean diameter as a function of dose are given in Figs. 5(b) and (c). The vacancy clusters were present in Mo irradiated at all doses from 7.2×10^{-5} to 0.28 dpa. Their size distribution was nearly unchanged during irradiation. The overall density of vacancy defects increased with dose by more than a factor of ten in the examined dose range with a tendency of leveling off at the highest dose. When the number density of cavities containing greater than 50 vacancies was plotted separately, the density increased from $\sim 10^{21}\ m^{-3}$ to $\sim 10^{23}\ m^{-3}$ as dose increased from 0.0072 dpa to 0.28 dpa. The number density of these large cavities in the 0.28 dpa specimen is comparable to the estimate from TEM observations. No such large cavities were observed in the 0.00072 dpa specimen, and the data point for the 7.2×10^{-5} dpa specimen cannot be explained. It is also noted that the cavity density follows a linear relation with neutron dose for 50-plus vacancy clusters and an exponent of ~ 0.5 for smaller vacancy clusters. The mean size of

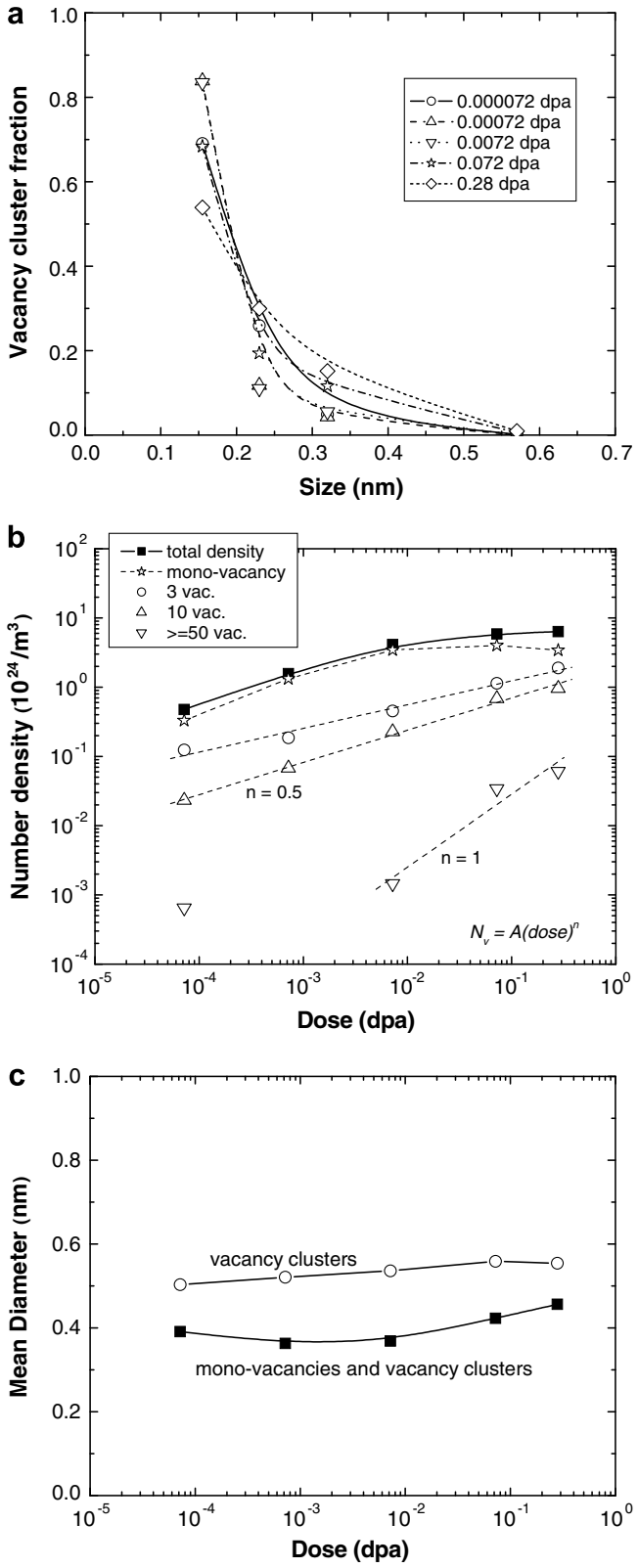

Fig. 5. (a) Size distribution, (b) dose dependence of number density, and (c) dose dependence of mean sizes of mono-vacancies and vacancy clusters in Mo neutron-irradiated at 80 °C.

vacancy clusters were calculated with and without including mono-vacancies, and the mean size showed only a small increase with dose, if any.

3.2. Post-irradiation tensile properties

3.2.1. Stress–strain behavior

The engineering stress–strain curves are shown in Fig. 6 for unirradiated and irradiated Mo tested over the temperature range of −50 to 100 °C at a nominal strain rate of 1×10^{-3} s^{-1}. Most of these results were reported previously [52]. The true stress–strain curves were calculated from the engineering stress–strain curves in the uniform elongation range, and they are given in Fig. 7. The yield point behavior, i.e. the upper and lower yield points and Lüders strain, was observed in the unirradiated specimens and specimens irradiated to low and intermediate doses (e.g. <0.01 dpa). The presence of the yield point and the magnitude of yield drop were dependent on both test temperature and neutron dose. The yield point was less evident as dose increased, and more pronounced as the test temperature decreased. The low and intermediate dose specimens also exhibited extensive strain hardening and uniform deformation at all test temperatures. The true uniform elongation was still about 10% at the test temperature of −50 °C. The plastic instability stress (PIS), i.e. the true stress at the ultimate tensile strength, was apparently independent of irradiation dose at a given test temperature (see Fig. 7). The strain hardening capacity of neutron-irradiated Mo was completely lost at doses >∼0.01 dpa, leading to the onset of plastic instability at yield and a nearly zero uniform elongation.

Fig. 8 shows the engineering stress–strain curves for unirradiated Mo and Mo irradiated to 0.003 and 0.029 dpa tested over the strain rate range of 1×10^{-5} to 1×10^{-2} s^{-1} at room temperature. The sensitivity of the yield point behavior to the strain rate is well-illustrated in Fig. 8(a) for unirradiated Mo and in Fig. 8(b) for Mo irradiated to 0.003 dpa. The upper and lower yield point and Luders elongation were more pronounced as the strain rate increased. Neutron irradiation reduced the yield point effect. Increasing strain rates increased the tensile strength and decreased the tensile ductility. Molybdenum irradiated to 0.029 dpa (Fig. 8(c)) showed completely brittle behavior even at a strain rate of 1×10^{-5} s^{-1}.

3.2.2. Tensile properties

Tensile properties, i.e. yield stress (YS), plastic instability stress (PIS), uniform elongation (UE), total elongation (TE) and reduction in area (RA) are shown in Fig. 9 in three-dimensional plots for irradiated Mo tested at a strain rate 1×10^{-3} s^{-1} between −50 and 100 °C to illustrate the dose and test temperature dependence of tensile properties. The yield stress was taken as the lower yield point when significant strain hardening and homogeneous deformation were observed; the yield stress was taken as the upper yield point when the onset of plastic instability at yield occurred.

As shown in Fig. 9(a), Mo experienced radiation-induced softening (decrease in yield stress) at lower doses when tested at low temperature; only radiation hardening (increase in yield stress) occurred at higher doses. The softening effect was stronger at lower test temperatures. No

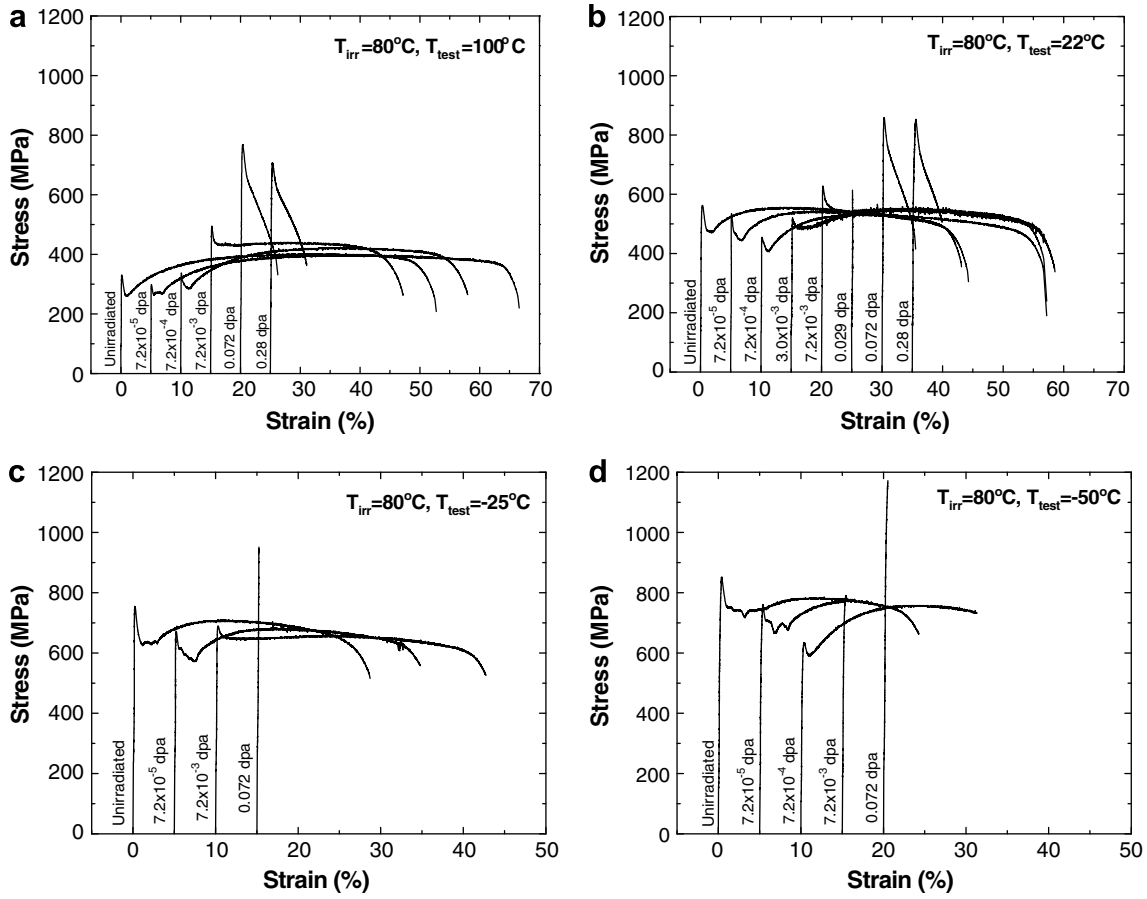

Fig. 6. Engineering stress–strain curves for Mo neutron-irradiated at 80 °C and tested at: (a) 100 °C, (b) 22 °C, (c) −25 °C and (d) −50 °C at a strain rate of 1×10^{-3} s^{-1}.

irradiation softening was observed by the tests at 100 °C. The softening effect was more evident in the 7.2×10^{-4} dpa specimen than in the 7.2×10^{-5} dpa specimen at a given test temperature, e.g. a 71 MPa drop in the yield stress at 7.2×10^{-5} dpa vs. 147 MPa drop at 7.2×10^{-4} dpa at the test temperature of −50 °C. When irradiation hardening occurred, the yield strength increased significantly with increasing dose up to ~0.1 dpa. Saturation or a decrease in the yield strength was observed above ~0.1 dpa. As described in the previous section, the PIS was not dependent on irradiation dose, while the PIS increased significantly with decreasing test temperature (shown in Fig. 9(b)). Note that the PIS is not defined when premature plastic instability at yield occurred.

Irradiation hardening was accompanied by a loss in ductility. As shown in Fig. 9(c), the uniform elongation was reduced to nearly zero at 0.072 dpa at all test temperatures, due to either plastic instability at yield at higher test temperatures or embrittlement at lower test temperatures. The critical dose for plastic instability at yield was ~0.072 dpa. When premature plastic instability occurred, the total elongation remained moderate (~5%) (see Fig. 9(d)) and the reduction in area was nearly unchanged within data scatter (see Fig. 9(e)). Embrittlement was more severe at lower test temperatures, and both the total elongation and reduction in area dropped dramatically.

The strain rate dependence of tensile properties is shown in Fig. 10 for Mo tested at room temperature. Increasing strain rates led to increases of both the yield stress and the PIS and decrease in ductility. The yield stress showed a stronger dependence on the strain rate than the PIS for unirradiated Mo. Irradiation to 0.003 dpa reduced the strain rate dependence of the yield stress, but had no impact on the magnitude and strain rate dependence of the PIS. The reduced strain rate dependence of the yield stress resulted in softening at higher strain rates, and hardening at lower strain rates in the 0.003 dpa specimens. The crossover of softening to hardening occurred at 3×10^{-3} s^{-1}. The strain rate dependence of the yield stress and the PIS was almost the same at 0.003 dpa. Both the yield stress, σ_{ys} and plastic instability stress, σ_{pis} exhibited a linear dependence on the strain rate, $\dot{\varepsilon}$ in semi-log scale, and the fitting of the YS data and the PIS data gave that:

$$\begin{aligned} \sigma_{ys}\ (\mathrm{MPa}) &= 711.3 + 82.3 \log \dot{\varepsilon} \quad \text{unirradiated}, \\ \sigma_{ys}\ (\mathrm{MPa}) &= 617.3 + 45.1 \log \dot{\varepsilon} \quad 0.003\ \text{dpa}, \\ \sigma_{pis}\ (\mathrm{MPa}) &= 775.5 + 43.9 \log \dot{\varepsilon} \end{aligned} \tag{1}$$

for both unirradiated and 0.003 dpa.

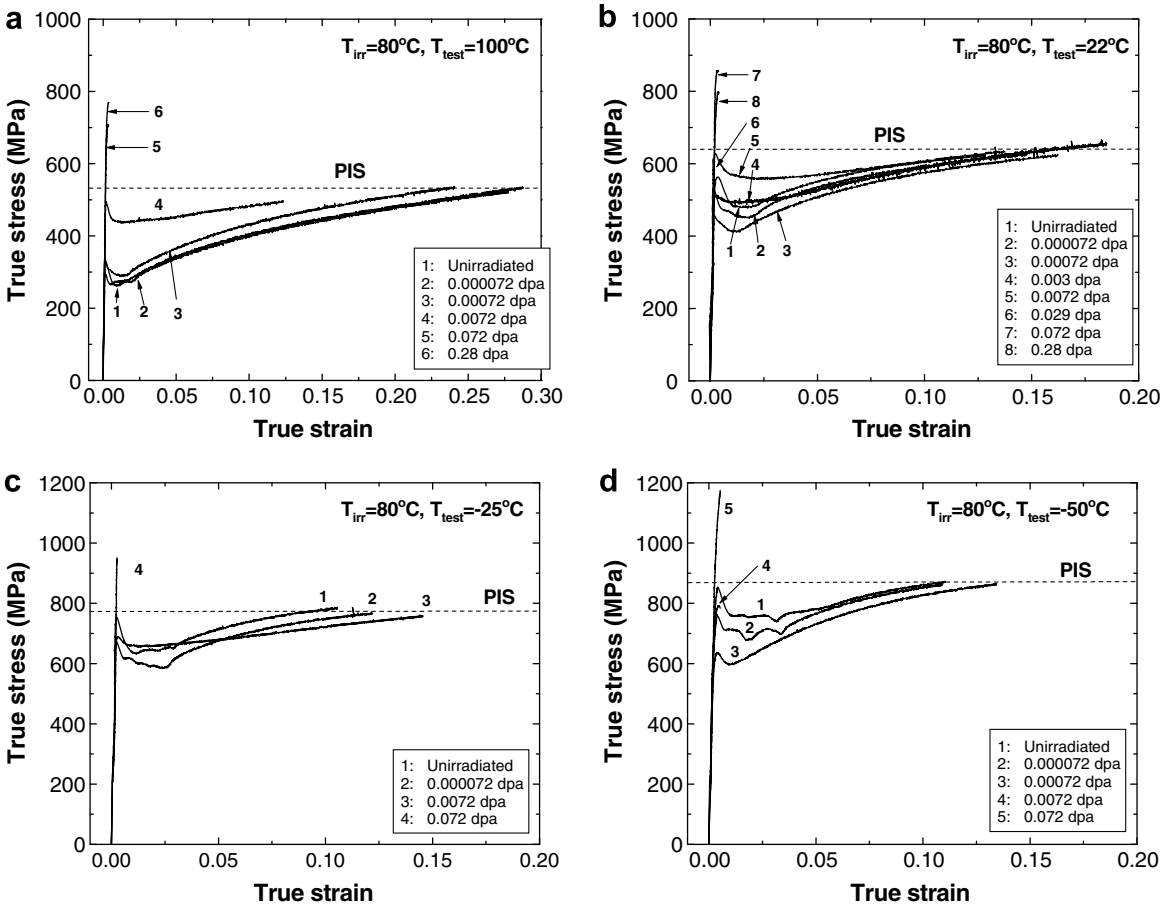

Fig. 7. True stress-strain curves for Mo neutron-irradiated at 80 °C and tested at: (a) 100 °C, (b) 22 °C, (c) −25 °C and (d) −50 °C at a strain rate of 1×10^{-3} s^{-1}.

The 0.029 dpa specimens exhibited completely brittle behavior at all strain rates.

3.3. Fractography of neutron-irradiated Mo

Fig. 11 shows SEM images of the fracture surfaces for Mo specimens neutron-irradiated to 7.2×10^{-5} dpa and tested at 1×10^{-3} s^{-1} between −50 and 100 °C. Their corresponding tensile curves are also shown in Fig. 11. The fracture mode at this dose level depends strongly on test temperature. A complete ductile, layered structure (delamination) was observed when the specimen was tested at 100 °C. As test temperature decreased, the fraction of areas exhibiting ductile failure decreased, and the amount of cleavage and grain boundary brittle fracture increased. At the test temperature of −50 °C, failure was solely by cleavage and (minor) grain boundary fracture.

A set of SEM fractographs and their corresponding tensile curves are shown in Fig. 12 for the specimens neutron-irradiated to 0.072 dpa. The dose dependence of fracture mode can be revealed by comparing Figs. 11 and 12. A significant difference in fracture mode was seen in the specimens tested at 22 °C. The 7.2×10^{-5} dpa specimen showed a dominant ductile fracture mode mixed with slight cleavage and grain boundary fracture, while the fracture mode in the 0.072 dpa specimen was dominated by cleavage fracture with a small fraction of layered, ductile fracture and grain boundary fracture.

3.4. Deformed microstructure of neutron-irradiated Mo

Representative TEM micrographs showing deformed microstructure in the uniform strain region of neutron-irradiated Mo are presented in Fig. 13 along with the corresponding engineering stress–strain curves. No dislocation channels were observed in the irradiated and tensile-deformed Mo specimens that exhibited extensive strain hardening. Only dislocation networks were observed in this case. Dislocation channels were observed in the 0.0072 dpa specimen tested at −50 °C when it failed at yield (0.24% plastic elongation) (micrograph shown in Fig. 13(a) and tensile curve indicated by No. 1 in Fig. 13(c)). The microstructure of this specimen consisted of nearly defect-free channels and undeformed regions containing a high number density of irradiation-induced defect clusters comparable to as-irradiated Mo. The channels were about 80 nm wide uniformly and the channel walls were smooth throughout the channel. Dislocation channels were also

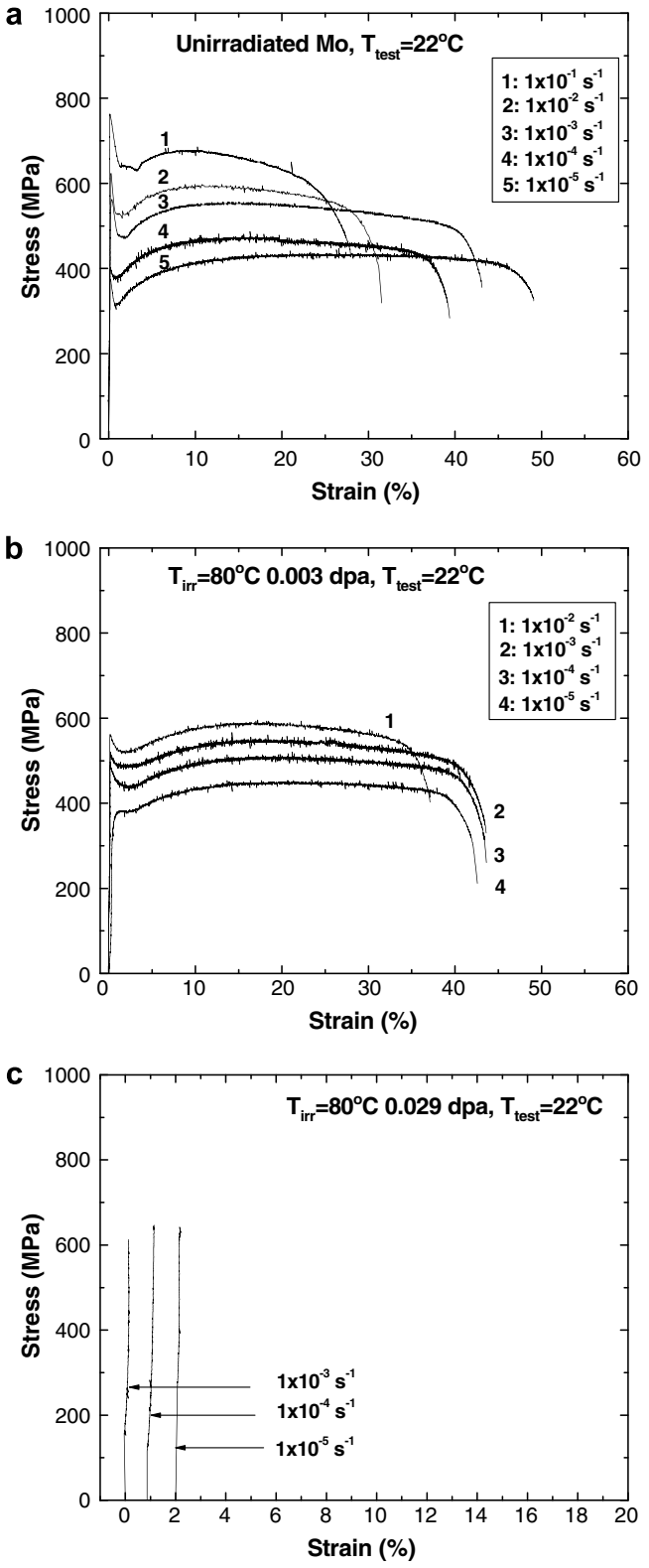

Fig. 8. Engineering stress–strain curves at various strain rates for Mo (a) unirradiated, (b) irradiated to 0.003 dpa, and (c) irradiated to 0.029 dpa tested at room temperature.

observed in the 0.072 dpa specimen tested at 22 °C (micrograph shown in Fig. 13(b) and tensile curve indicated by No. 2 in Fig. 13(c)). Channels were cleared of defects with a few residual dislocations and debris from partially annihilated defect clusters. The width of channels varied (60–160 nm). Compared to the as-irradiated microstructure, the deformed matrix had a high density of dislocation lines decorated with dislocation loops. Rafts seen in the as-irradiated specimens were still present in irradiated and deformed Mo. In general, thinner channels were observed at a lower test temperature. Due to the limited thin area in these specimens, complete quantitative characterization of channels could not be performed.

4. Discussion

4.1. Formation of radiation-induced defect clusters

Microstructural evolution in Mo neutron-irradiated at low doses at low temperature has been characterized by TEM, PAS and room-temperature electrical resistivity. Both dislocation loops and cavities were detected. The TEM-visible dislocation loops are assumed to be predominantly interstitial-type according to previous loop analyses of neutron-irradiated Mo in the literature [45–50]. Several salient characteristics of defect clusters are summarized as follows: (1) defect clusters were not visible by TEM at a very low dose of ~0.0001 dpa; (2) the number density of visible defect clusters increased with increasing dose in a sublinear manner, reached a maximum at ~0.03 dpa and decreased with continuous increase of dose, (3) the mean size of visible defect clusters increased from 1.94 to 3.36 nm as dose increased, and the size distribution was broader at higher doses; (4) there was a strong indication of aggregation of dislocation loops and formation of rafts at higher doses; (5) cavities were detected by PAS at all doses between 7.2×10^{-5} and 0.28 dpa; (6) the mean size of cavities increased only slightly (if any) with increasing doses; (7) weak contrast of cavities were observed by TEM only in the highest dose (0.28 dpa) specimen; (8) the estimated cavity density ($\sim 10^{23}$ m^{-3}) by TEM is comparable to the density of cavities containing more than 50 vacancies detected by PAS; (9) there was no measurable increase in room-temperature electrical resistivity at a very low dose of ~0.0001 dpa, and the electrical resistivity increased continuously with increasing dose up to 0.28 dpa.

The microstructural features of dislocation loops and rafts are consistent with those observed in previous studies of neutron-irradiated Mo at comparable irradiation temperatures. The defect cluster density was relatively low in the present experiments compared to the results reported by Tanaka et al. [9] and by Niebel and Wilkens [43] on polycrystalline Mo (see Fig. 3). All three studies showed a continuous increase in number density below 0.03 dpa, while the decrease in density and size with further irradiation was more gradual in this study than that observed by Tanaka et al. The accumulation rate of visible defect clusters reported by Niebel et al. was noticeably smaller than all other studies due to the very high cluster density at low doses. The material purity could be a major factor that

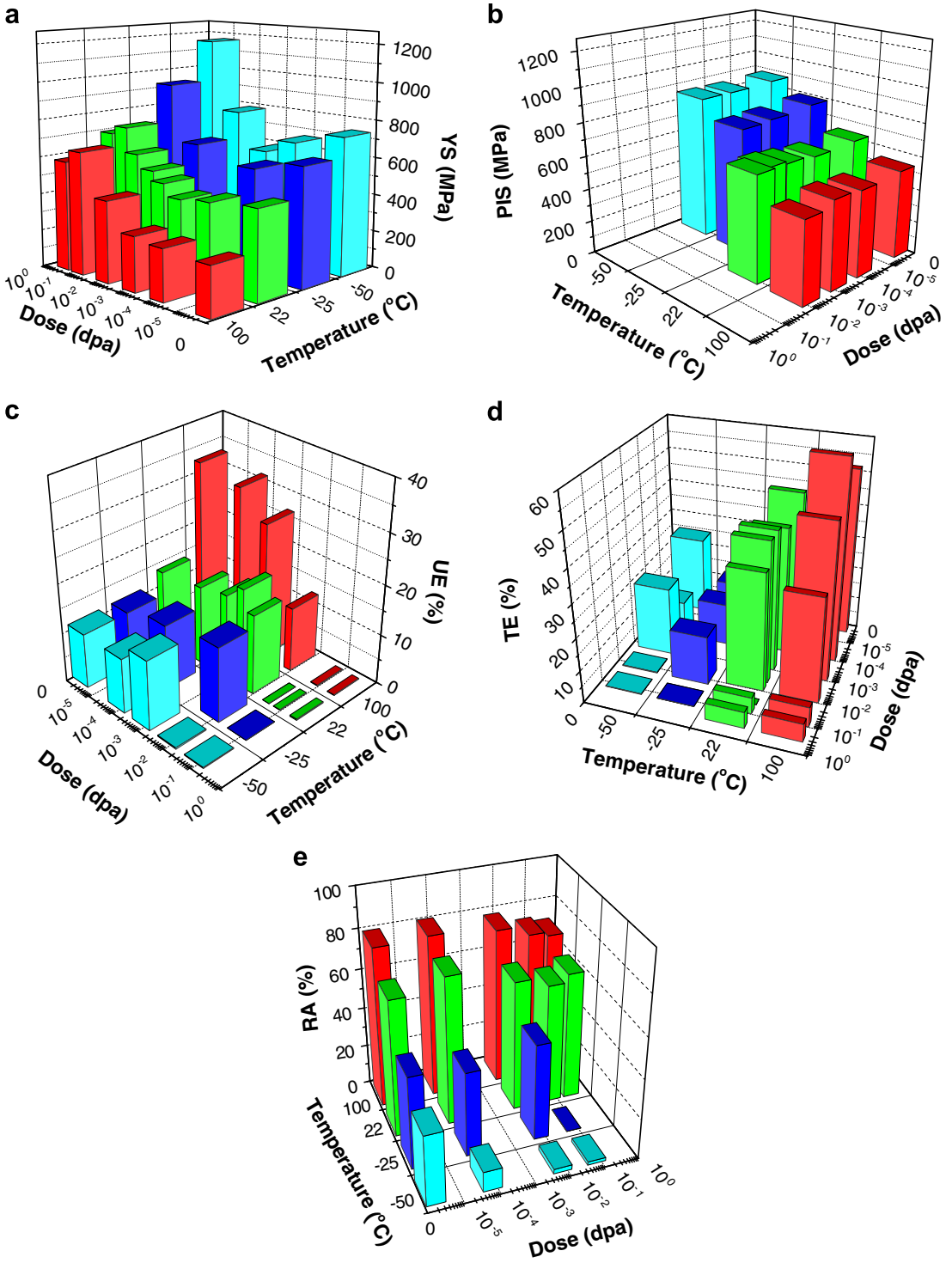

Fig. 9. Dose and temperature dependence of (a) yield stress (YS), (b) PIS, (c) uniform elongation (UE), (d) total elongation (TE) and (e) reduction in area (RA) for unirradiated and irradiated Mo tested at a strain rate 1×10^{-3} s^{-1} between −50 and 100 °C.

contributes to the variations in visible defect cluster density among different studies. The effect of impurity trapping of self-interstitial atoms (SIA) in Mo has been demonstrated by Eyre et al. [47], where the visible clusters were significantly finer in low purity Mo.

The trends of cluster density and size changes with dose for polycrystalline Mo in the present study are comparable to the results on mono-crystalline Mo by Singh et al. [10]. However, the cluster density in polycrystalline Mo was nearly one order of magnitude higher, and the mean sizes of defect clusters were about a half that found in mono-crystalline Mo. Raft formation was observed at doses about 0.01 dpa and higher in both the mono-crystalline and polycrystalline Mo. Comparing pure Mo and Mo

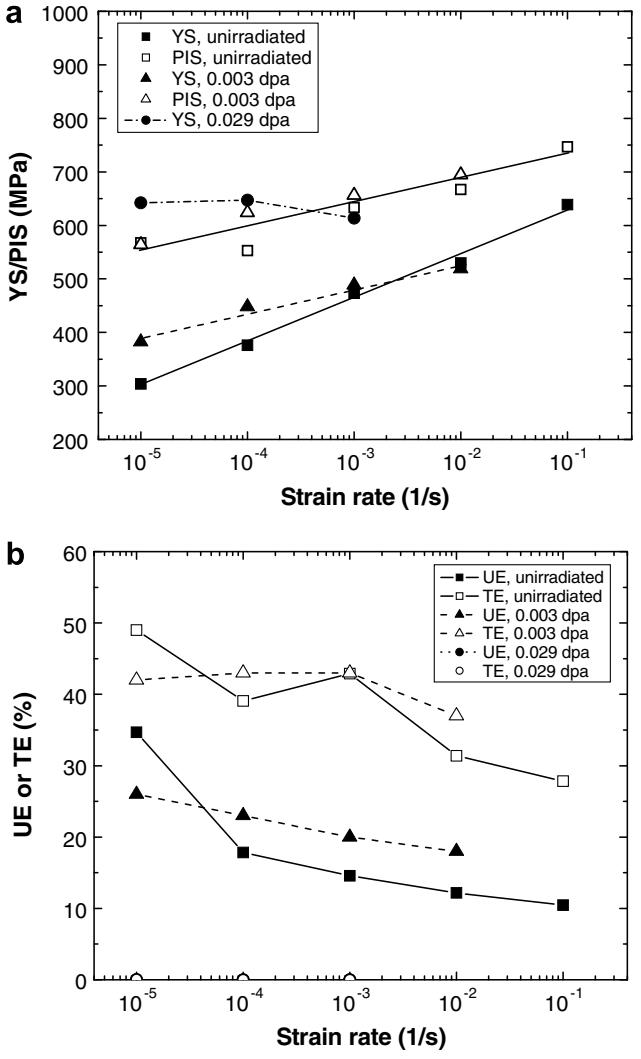

Fig. 10. Strain rate dependence of (a) the yield stress (YS) and PIS and (b) uniform elongation (UE) and total elongation (TE) for unirradiated and irradiated Mo tested at room temperature. The 0.029 dpa specimens showed premature brittle failure.

alloys, the cluster density in Mo–Re and TZM alloys was higher, and the cluster size increased more rapidly with increasing dose [10,11,44]. Singh et al. [10,11] reported a decreased cluster density with increasing dose in the intermediate and high dose regime for neutron-irradiated Mo–Re and TZM alloys, while Muller [44] showed a nearly constant defect cluster density in Mo-Re and TZM alloys under 600 MeV proton irradiation. It appears that the addition of alloying elements affects the nucleation rate and mobility of defect clusters.

It is informative to compare the irradiated microstructure between medium-mass bcc Fe and high-mass bcc Mo neutron-irradiated near room temperature. The same types of defect structure, i.e. dislocation loops, rafts and cavities, were observed in these two bcc metals [16,51]. Fig. 14 compares the dose dependence of loop and cavity densities and their mean sizes in Mo and Fe following neutron irradiation at 60–80 °C. The Fe data were taken from the Refs. [16,51]. No visible dislocation loops were observed in either Mo or Fe at a very low dose (~0.0001 dpa) where displacement cascades were largely separated. The threshold dose for visible loops was similar in both metals, ~0.0007–0.0008 dpa. However, the loop density in neutron-irradiated Mo was about one order of magnitude higher than in Fe at 0.001 dpa, $\sim 2 \times 10^{22}\,m^{-3}$ in Mo vs. $\sim 1 \times 10^{21}\,m^{-3}$ in Fe. The accumulation rate of visible loops in Mo and Fe was similar up to about 0.03 dpa where the loop density in Mo reached a maximum and yet the loop density in Fe increased continuously with increasing dose up to ~1 dpa. The cavity density is also slightly higher in Mo than in Fe. The mean size of loops in Mo were larger than in Fe at low doses but the loop size in Fe increased much more rapidly with dose than in Mo. The cavity size in Fe also showed an evident increase, but not in irradiated Mo.

The lack of TEM-visible dislocation loops at a very low dose indicated that large, sessile self-interstitial atoms (SIA) clusters were not produced directly in displacement cascades. Homogeneous nucleation and growth is insufficient to form visible defect clusters at this low dose due to its low rate and widely separated cascades. The sublinear defect accumulation behavior revealed by the dose dependence of visible loop density and the loop size dependence upon dose at intermediate doses further indicate that the visible interstitial loops were not formed by in-cascade clustering. Significant raft formation in Mo at higher doses may be explained by diffusional glide of small SIA clusters produced in displacement cascades, which also explains the decreased number density of visible defect clusters at higher doses (>0.03 dpa). The reduced cluster density could be due to destruction of pre-existing defects by cascade overlapping as well. Molecular dynamic simulations [20] have found significant in-cascade interstitial clustering in irradiated Mo with a majority of interstitial defect clusters composed of only a few defects. These interstitial clusters take the form of $\frac{1}{2}\langle 111\rangle$ primatic loop embryos and most are glissile at room temperature. Only a very low fraction of clusters is in sessile configurations. A high number density of large, sessile dislocation loops visible by TEM must be formed by both interactions between small glissile interstitial defects and through diffusive nucleation and growth processes during irradiation, similar to the cluster formation process in irradiated Fe [16]. Despite the fact that the point defect nucleation and growth is dominant in the formation of large, sessile interstitial clusters in both Mo and Fe, the higher number density and larger mean size of visible defect clusters at low doses in Mo imply that in-cascade interstitial clustering in Mo may be more significant than in Fe.

The findings of cavities in neutron-irradiated Mo at such a low irradiation temperature, 80 °C (0.12 T_m, where T_m is the melting point) in the present study are of great significance. It is noted that the irradiation temperature is considerably lower than the Mo recovery stage III temperature, 150–200 °C (0.15–0.16 T_m) when vacancy migration occurs [53,54]. Positron annihilation spectroscopy detected cavi-

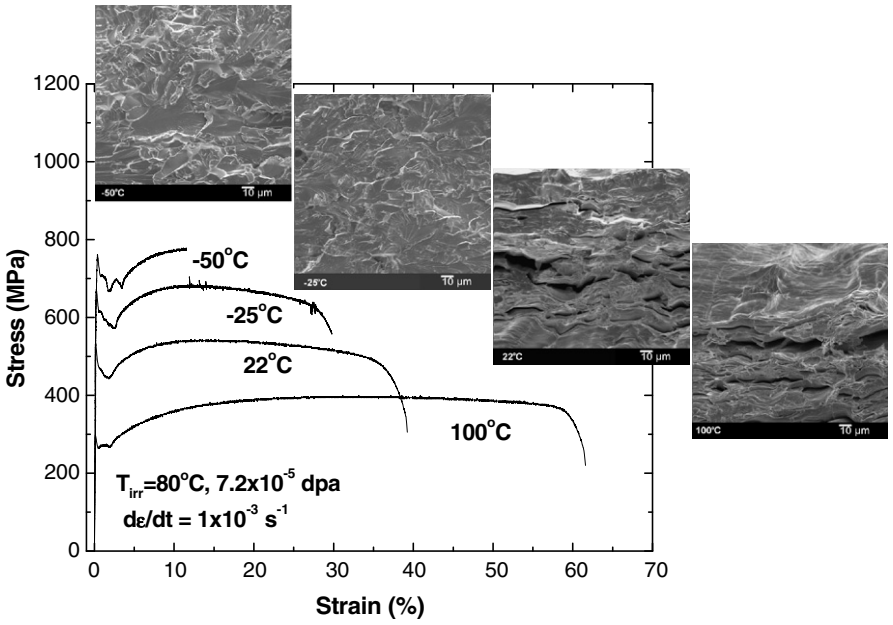

Fig. 11. Fractography for Mo neutron-irradiated to 7.2×10^{-5} dpa and tested at 1×10^{-3} s^{-1} between −50 and 100 °C.

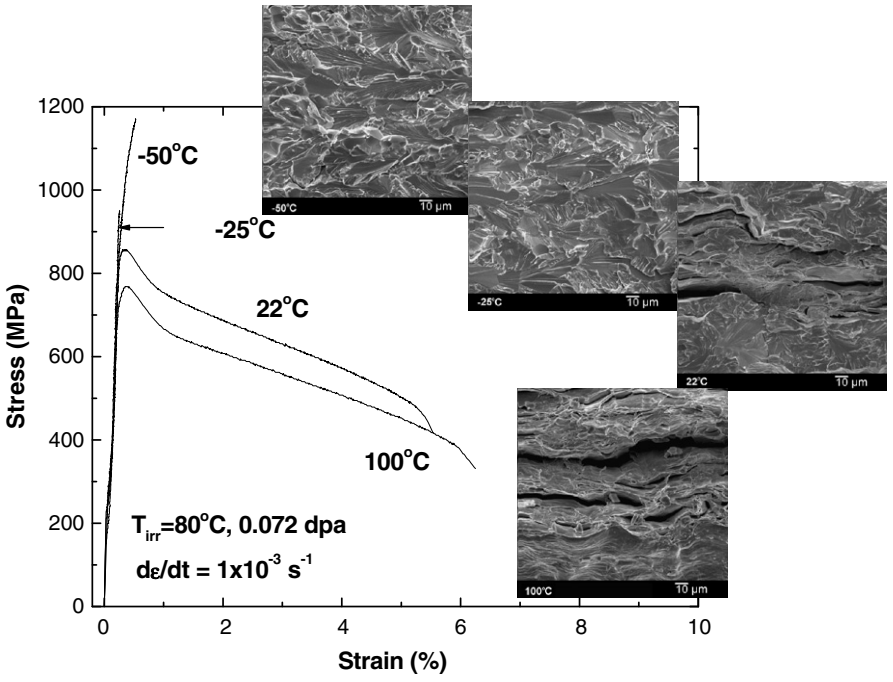

Fig. 12. Fractography for Mo neutron-irradiated to 0.072 dpa and tested at 1×10^{-3} s^{-1} between −50 and 100 °C.

ties in Mo at a dose as low as ~0.0001 dpa, similar to the threshold dose in neutron-irradiated Fe [51]. The cavity densities in Mo is slightly higher than in Fe, and the average size of cavities in Mo is relatively insensitive to the neutron dose as opposed to an evident increase in cavity mean size with dose in Fe, as shown in Fig. 14 [16,51]. What is more important is that the size distribution of vacancy cluster in Mo remained nearly constant with the peak at the size of mono-vacancy, while the size distribution tends to shift with the peak at the increasing size with increasing dose in Fe [51]. These observations suggest that in-cascade vacancy clustering is more significant in Mo than in Fe, which is supported by MD computer simulations [20,21]. The increased tendency of in-cascade vacancy clustering in Mo was also supported by the findings of higher defect yield (ratio of the number of visible vacancy loops and the number of cascades generated per unit area) and cascade efficiency (ratio of the number of vacancies retained in a loop of average area and the calculated number of vacancies generated in the cascade) in Mo as compared to Fe

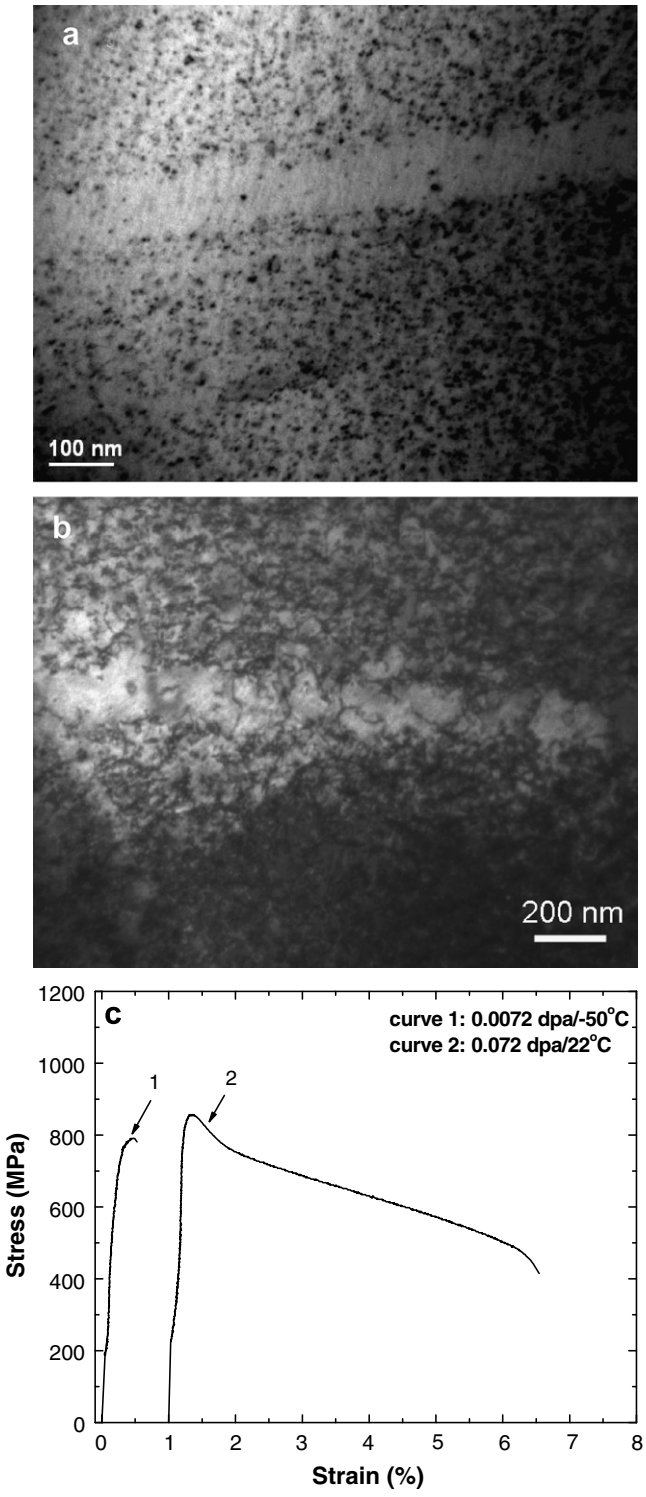

Fig. 13. Deformed microstructure and their corresponding stress–strain curves for neutron-irradiated Mo (a) micrograph for the 0.0072 dpa/−50 °C specimen, (b) micrograph for the 0.072 dpa/22 °C specimen, (c) stress–strain curves of the 0.0072 dpa/−50 °C specimen and the 0.072 dpa/22 °C specimen.

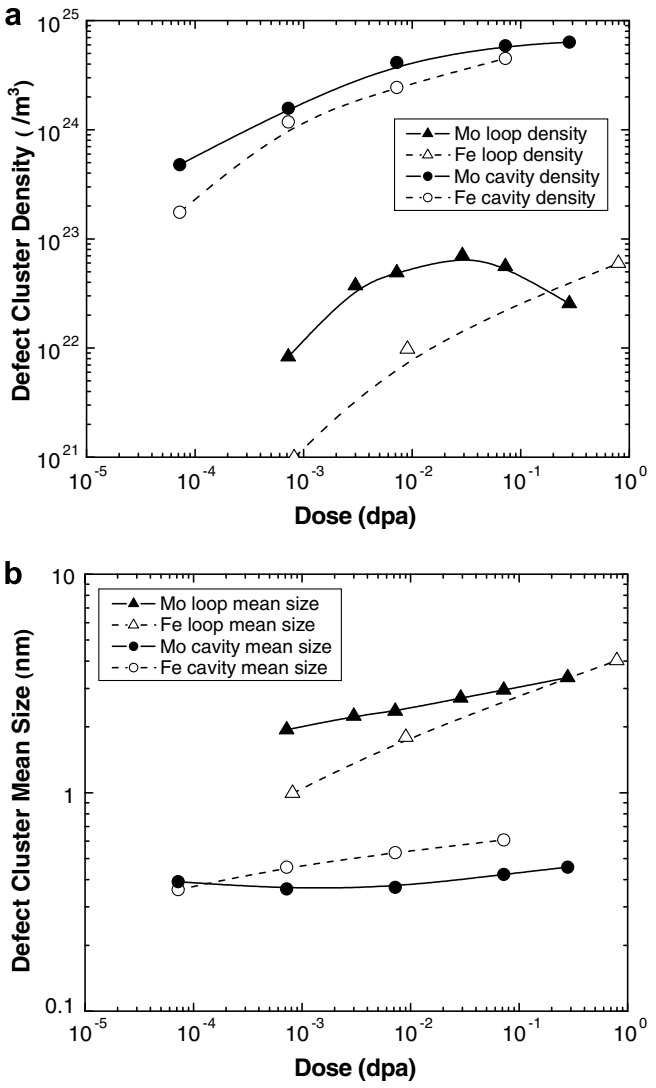

Fig. 14. Comparison of dose dependence of loop and cavity density (a) and mean size (b) in Mo and Fe irradiation at 60–80 °C. The Fe data were taken from Refs. [16,51].

in heavy-ion irradiation experiments [12,13]. The average defect yield and cascade efficiency was 0.12 and 0.36, respectively for Mo irradiated with 60 keV self-ions at room temperature, and yet no visible damage seen in bcc Fe when irradiated with 80 keV self-ions. Although a majority of vacancy clusters predicted by MD simulations had the sizes below TEM visibility limit, vacancy clusters as large as 60 defects were produced in a 50 keV cascade energy, and these sizeable clusters were considerably larger in Mo as compared to bcc Fe [20,21]. The morphology of vacancy clusters observed in the present experiment is consistent with the predictions by MD simulations, i.e. all the largest vacancy clusters are compact, three-dimensional objects.

4.2. Radiation softening and hardening

A strong effect of neutron irradiation on the yield stress was found in Mo. The dose dependence of the change in yield stress clearly indicated three dose regimes (see Fig. 15): (1) radiation-induced yield softening ($\Delta\sigma_{YS} < 0$) at lower doses ($<\sim$0.003 dpa), (2) radiation-induced yield

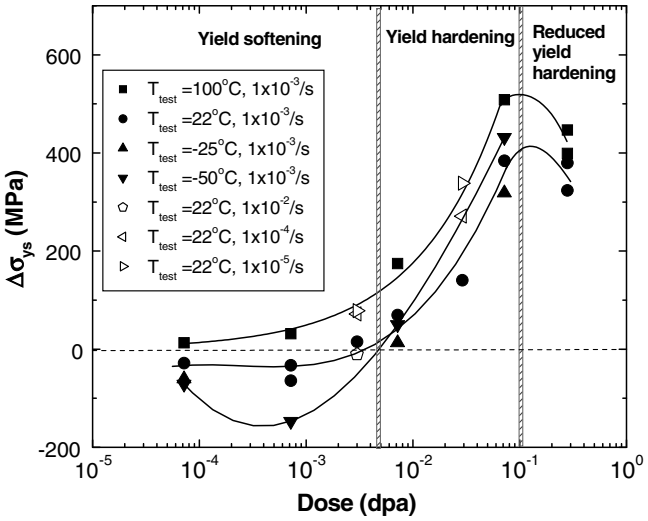

Fig. 15. The change in the yield stress of neutron-irradiated Mo tested between −50 and 100 °C.

hardening ($\Delta\sigma_{YS} > 0$) at intermediate doses (~0.003–0.1 dpa), (3) reduced radiation hardening ($\Delta\sigma_{YS} > 0$ and $d\Delta\sigma_{YS}/d(\text{dose}) < 0$) at higher doses (~>0.1 dpa). The cross-over of softening to hardening was dependent on the test temperature and the strain rate. The softening effect was stronger at a lower test temperature and a higher strain rate. The relation $\Delta\sigma_{YS} = A(\phi t)^{1/2}$ where (ϕt) is the neutron fluence, and A is a constant, holds up to ~0.1 dpa if $\Delta\sigma_{YS}$ is taken as the increase in athermal stress of the yield stress after irradiation.

Neutron irradiation had a pronounced effect on the temperature and strain rate dependence of the yield stress in Mo as well (strain rate dependence shown in Fig. 10(a) and temperature dependence shown in Fig. 16). As opposed to some irradiated fcc metals where the temperature dependence of the yield stress is markedly increased after neutron irradiation [22,55], the temperature and strain rate dependence of the yield stress in Mo was reduced by neutron irradiation. The temperature and strain rate dependence of the yield stress decreased as dose increased up to ~0.003 dpa, above which the temperature and strain rate dependence of the yield stress remained nearly constant during further irradiation. It is interesting to note the temperature dependence of the yield stress was stronger than that of the PIS in unirradiated Mo. Neutron irradiation had no effect on the magnitude and temperature dependence of the PIS, while irradiation reduced the temperature dependence of the yield stress to nearly the same level as the PIS before athermal hardening occurred.

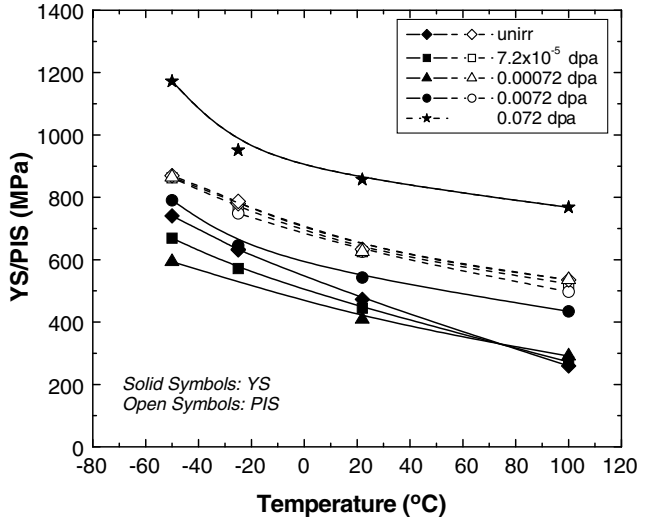

Fig. 16. Temperature dependence of the yield stress (YS) and the plastic instability stress (PIS) for unirradiated and irradiated Mo tested between −50 and 100 °C.

Significant radiation softening and reduced test temperature and strain rate dependence of the yield stress at lower doses implies that radiation-induced defect clusters are mainly short-range thermal barriers to dislocation motion, affecting the rate-controlling deformation mechanism at low temperatures. Previous analysis [52] showed that irradiation-induced defects in Mo that account for short-range barriers are in agreement with the Fleischer theory and they were mainly submicroscopic defects. A possible explanation for the reduced temperature dependence of the yield stress could be due to trapping of interstitial solutes in point defect-impurity complexes.

The absence of a change in the temperature dependence of the yield stress upon further irradiation (>~0.003 dpa) implies that irradiation-produced obstacles to dislocation motion are largely athermal in nature [23]. A high number density of visible dislocation loops may account for these long-range barriers. This again suggests that large, sessile defect clusters (athermal hardening centers) formed primarily through reactions between randomly diffusing mobile defects. The hardening effect from large, sessile defect clusters may be understood using dispersed barrier hardening models [56]. The barrier strength of defect clusters can be determined by correlating the athermal stress and the measured density and size of defect clusters [42,52]. The calculated value of barrier strength, α for visible defect clusters and large size cavities (containing 50 vacancies) increased from 0.1 to 0.3–0.4 as doses increased from 0.003 to 0.3 dpa.

4.3. Plastic instability and fracture

As observed in several irradiated bcc metals [32], plastic instability at yield (PIS = YS) occurs in Mo after irradiation to about 0.01–0.1 dpa, depending on the test temperature and the strain rate. Below this critical dose for plastic instability, the engineering stress–strain curves consist of a few distinct regions including elastic strain, yield drop, Luders strain, strain hardening, and necking; above the critical dose, the curves show prompt ductile necking or complete brittleness. The prompt plastic instability has been associated with the increase in yield stress and the loss of strain hardening capacity in irradiated metals [32–35,57,58]. It was shown in several fcc and bcc metals that

the true strain hardening behavior is dose-independent [32,35]. The dose-independence of strain hardening was also observed in the present study on Mo, as shown in Fig. 17, where the true stress-true strain curves for the neutron-irradiated Mo are superimposed on the unirradiated curve by shifts in the negative or positive direction of the strain axis depending on the dose and its consequent softening and hardening behavior. It holds true for not only the true stress-strain curves tested at different temperature but also those tested at varied strain rates. Likewise, the insensitivity of the PIS to neutron dose was also confirmed in neutron-irradiated Mo. The implication of irradiation-insensitive strain hardening is that one constitutive stress-strain relation may be applied to both unirradiated and irradiated conditions.

Dislocation channels were observed only in the medium and higher dose specimens (>~0.01 dpa) that exhibited premature plastic instability or embrittlement. Dislocation channeling was not observed in specimens that deformed uniformly. Dislocation channels were also observed in irradiated Mo in earlier work [59–61]. However, no definite correlation between dislocation channeling and prompt plastic instability can be established for irradiated Mo. It is apparent that the local strain level, test temperature and the stress state are important factors that affect characteristics of dislocation channeling. An undeformed matrix with a high density of defect clusters and defect-free channels was observed in the 0.0072 dpa/−50 °C specimen at a uniform strain of 0.24%, while a highly-deformed matrix with dislocation networks together with defect-free channels was observed in the 0.072 dpa/22 °C specimen. In either case, an increased defect cluster density along the channel edges was not observed, which rules out the mechanism of the 'snow-plough' removal of defects [62]. The observation of channels at −50 °C implies that a diffusion-controlled mechanism for defect removal is not important in irradiated Mo [62]. The reduction in channel width at a lower deformation temperature suggests that the cross slip of the screw dislocations may be an important factor in the formation of dislocation channels in Mo [63].

Three fracture modes were observed in neutron-irradiated Mo: layered ductile fracture, cleavage fracture and grain boundary brittle fracture. The fracture mode is more dependent on test temperature and radiation hardening rather than strain localization. Fig. 18 maps out fracture modes at a given test temperature and neutron dose in terms of temperature dependence of the PIS, upper yield stress (UPS) (for specimens exhibiting plastic instability at yield) and fracture stress (FS) for Mo. The fracture stress was calculated by the final fracture load and the final cross-section area. The fracture mode is most sensitive to test temperature, radiation hardening has secondary importance and strain localization has little influence on fracture modes. In fact, premature necking at yield does not seem to affect the amount of necking strain or reduction of area, as shown in

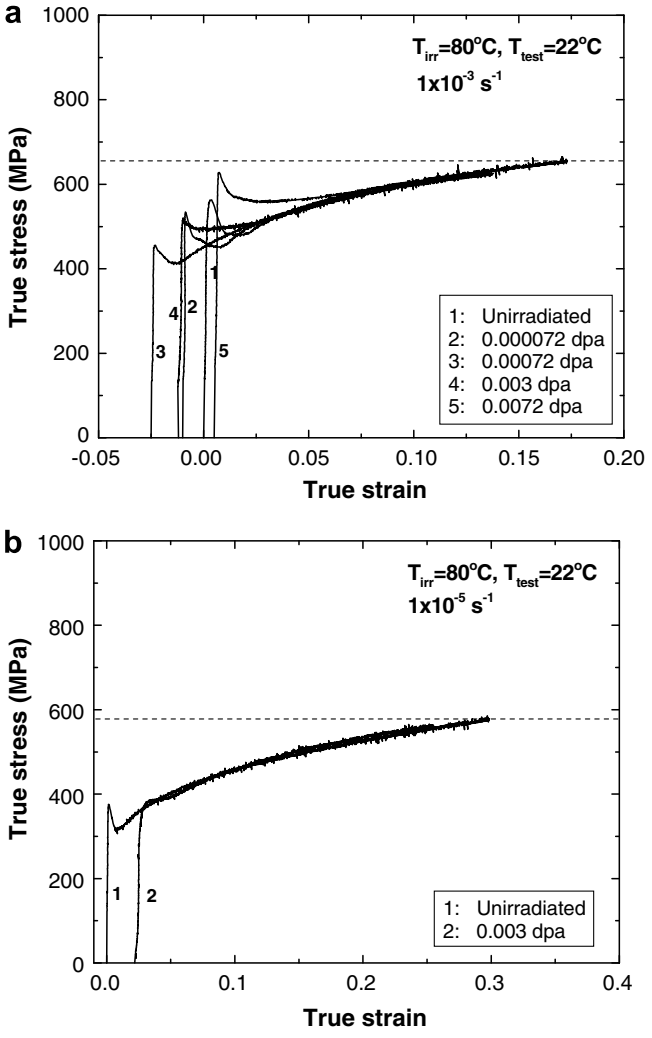

Fig. 17. True stress–strain curves for Mo neutron-irradiated at 80 °C and tested at 22 °C (a) strain rate 1×10^{-3} s^{-1} and (b) strain rate 1×10^{-5} s^{-1}. The curves are superimposed on the unirradiated curve by shifting along the strain axis.

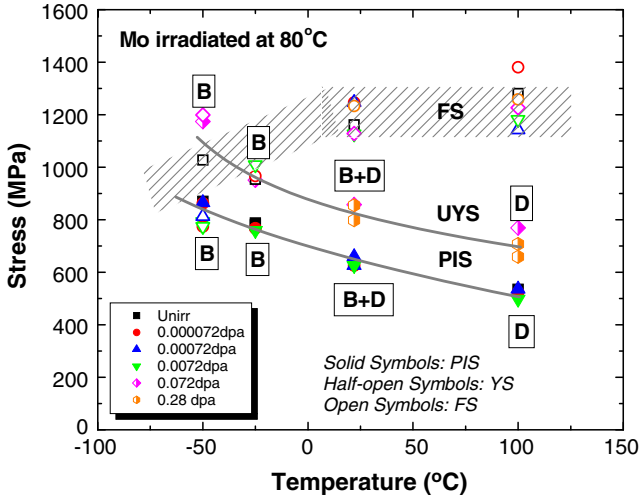

Fig. 18. Plastic instability stress (PIS), upper yield stress (UYS), and fracture stress (FS) as a function of test temperature for unirradiated and irradiated Mo. The fracture modes are marked (D – ductile fracture, B – brittle fracture).

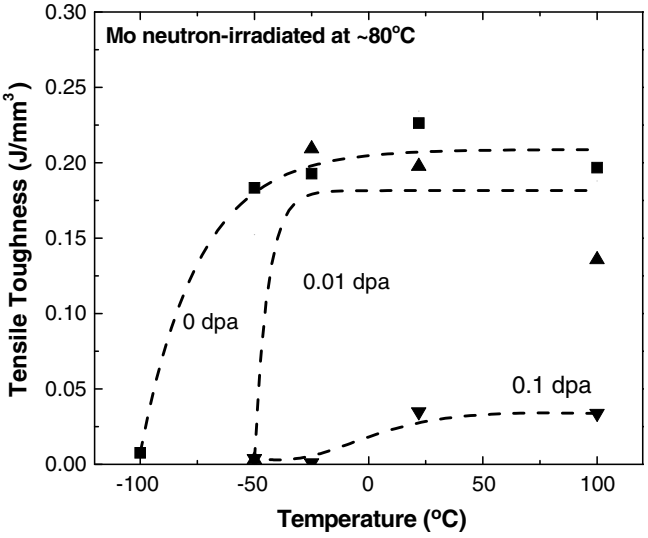

Fig. 19. Tensile toughness vs. test temperature for unirradiated and irradiated Mo. The tensile toughness is defined as the area of the stress–strain curve which corresponds to the dimension of the energy per unit volume.

Fig. 9(e). The irradiation-induced loss of strain hardenability may be responsible for the decrease in tensile toughness. As shown in Fig. 19, where the tensile toughness is calculated by integrating the engineering stress–strain curves, neutron irradiation caused an increase in tensile DBTT and a large reduction in upper shelf tensile toughness that is associated with premature plastic instability and ductility loss.

No direct correlation between dislocation channeling and brittle fracture in neutron-irradiated Mo could be confirmed in these experiments. In fact, the specimen that exhibited channeling failed in a completely ductile manner, and the specimen that showed extensive uniform deformation showed cleavage fracture. Significant irradiation hardening seems to be a major cause of irradiation embrittlement at low temperatures. It has been found that the cleavage fracture stress of a material is insensitive to neutron irradiation [64]. The calculated fracture mechanism map of irradiated Mo has shown that the cleavage fracture field is enlarged after irradiation due to the insensitivity of intrinsic cleavage fracture stresses to neutron irradiation and irradiation-induced increase in the yield stress [64]. The transition temperature from brittle to ductile fracture shifted from 0.09 T_m for unirradiated Mo to 0.14 T_m for irradiated Mo in the calculated map.

5. Conclusions

The important findings from this study are summarized as follows:

(1) The major types of irradiation-induced defect structure in Mo were dislocation loops, rafts and cavities. The threshold for visible dislocation loops by TEM was ~0.001 dpa, and the loop density maximum was at 0.03 dpa. Raft formation became evident at ~0.01 dpa. Cavities were detectable by PAS at all doses between 7.2×10^{-5} and 0.28 dpa. The mean size of vacancy cavities was about 0.5–0.6 nm. Both the mean size and size distribution of cavities were relatively insensitive to neutron dose. The formation of sessile interstitial defect clusters in Mo is suggested to be dominated by homogeneous nucleation and growth. In-cascade vacancy clustering appears to be more significant in Mo than in bcc Fe.

(2) Neutron irradiation has a pronounced effect on the yield stress of Mo. Irradiation at lower doses reduced the temperature and strain rate dependence of the yield stress, leading to softening at a lower test temperature and at a higher strain rate. The crossover of softening and hardening is related to the test temperature and the strain rate. Further irradiation gave rise to athermal hardening only. An apparent saturation or reduced magnitude of irradiation hardening occurred at >~0.1 dpa.

(3) The magnitude and the temperature and strain rate dependence of the PIS was apparently not affected by neutron irradiation. The temperature and strain rate dependence of the yield stress was reduced by irradiation to the same level as of the PIS before athermal hardening took place.

(4) Significant irradiation hardening was accompanied by premature necking at yield and embrittlement. Dislocation channeling was observed in the specimens that showed premature necking at yield. However, no direct correlation between dislocation channels and premature plastic instability can be established.

(5) Ductile laminar fracture and transgranular cleavage mixed with intergranular brittle fracture were observed in irradiated Mo. Brittle fracture is primarily dependent on the test temperature and the strain rate, and the magnitude of irradiation hardening. There is no apparent connection between dislocation channeling and embrittlement.

Acknowledgements

The research was sponsored by the Office of Fusion Energy Sciences, the US Department of Energy under contract DE-AC05-00OR22725 with Oak Ridge National Laboratory, managed and operated by UT-Battelle, LLC. The authors would like to thank Dr R.E. Stoller for his valuable input. We would also like to thank J.L. Bailey, A.M. Williams, L.T. Gibson and P.S. Tedder for their technical support.

References

[1] T.H. Webster, B.L. Eyre, E.A. Terry, Irradiation Embrittlement and Creep in Fuel Cladding and Core Components, The British Nuclear Energy Society, London, 1972.

[2] B.V. Cockeram, J.L. Hollenbeck, L.L. Snead, J. Nucl. Mater. 324 (2004) 77.
[3] B.V. Cockeram, R.W. Smith, L.L. Snead, J. Nucl. Mater. 346 (2005) 145.
[4] I.V. Gorynin, V.A. Ignatov, V.V. Rybin, S.A. Fabritsiev, et al., J. Nucl. Mater. 191–194 (1992) 421.
[5] K. Furuya, J. Moteff, J. Nucl. Mater. 99 (1981) 306.
[6] K. Watanabe, A. Hishinuma, Y. Hiraoka, T. Fujii, J. Nucl. Mater. 258–263 (1998) 848.
[7] A. Hasegawa, K. Abe, M. Satou, K. Ueda, C. Namba, J. Nucl. Mater. 233–237 (1996) 565.
[8] G.V. Muller, D. Gavillet, M. Victoria, J.L. Martin, J. Nucl. Mater. 212–215 (1994) 1283.
[9] M. Tanaka, K. Fukaya, K. Shiraishi, Trans. JIM 20 (1979) 697.
[10] B.N. Singh, J.H. Evans, A. Horsewell, P. Toft, G.V. Műller, J. Nucl. Mater. 258–263 (1998) 865.
[11] B.N. Singh, J.H. Evans, A. Horsewell, P. Toft, D.J. Edwards, J. Nucl. Mater. 223 (1995) 95.
[12] C.A. English, M.L. Jenkins, Mater. Sci. Forum 15–18 (1987) 1003.
[13] M.L. Jenkins, M.A. Kirk, W.J. Phythian, J. Nucl. Mater. 205 (1993) 16.
[14] S.J. Zinkle, B.N. Singh, J. Nucl. Mater. 199 (1993) 173.
[15] S.J. Zinkle, Y. Matsukawa, J. Nucl. Mater. 329–333 (2004) 88.
[16] S.J. Zinkle, B.N. Singh, J. Nucl. Mater. 351 (2006) 269.
[17] Y. Zhong, K. Nordlund, M. Ghaly, R.S. Averback, Phys. Rev. B 58 (1998) 2361.
[18] W.J. Phythian, R.E. Stoller, A.J.E. Foreman, A.F. Calder, D.J. Bacon, J. Nucl. Mater. 223 (1995) 245.
[19] M.J. Caturla, N. Soneda, E. Alonso, B.D. Wirth, T. Díaz de la Rubia, J.M. Perlado, J. Nucl. Mater. 267 (2000) 13.
[20] P. Pasianot, M. Alurralde, A. Almazouzi, M. Victoria, Phil. Mag. A 82 (2002) 1671.
[21] R.E. Stoller, G.R. Odette, B.D. Wirth, J. Nucl. Mater. 251 (1997) 49.
[22] T.J. Koppenaal, R.J. Arsenault, Metall. Rev. 157 (1971) 175.
[23] E.A. Little, Int. Metals Rev. 21 (1976) 25.
[24] M.S. Wechsler, Defects in Refractory Metals, 1971, p. 257.
[25] M.S. Wechsler, R.P. Tucker, R. Bode, Acta Metall. 17 (1969) 541.
[26] P.R.V. Evans, A.F. Weinberg, R.J. Van Thyne, Acta Metall. 11 (1963) 143.
[27] G.R. Smolik, C.W. Chen, J. Nucl. Mater. 35 (1970) 94.
[28] H. Matsui, H. Shimidzu, S. Ta, M.W. Guinan, J. Nucl. Mater. 155–157 (1988) 1169.
[29] R.J. Arsenault, E. Pink, Mater. Sci. Eng. 8 (1971) 141.
[30] K. Kitajima, H. Abe, Y. Aono, E. Kuramoto, J. Nucl. Mater. 108&109 (1982) 436.
[31] G. Dieter, Mechanical Metallurgy, third ed., McGraw-Hill Science/Engineering/Math, 1986.
[32] T.S. Byun, K. Farrell, Acta Mater. 52 (2004) 1597.
[33] T.S. Byun, N. Hashimoto, K. Farrell, Acta Mater. 52 (2004) 3889.
[34] X. Wu, X. Pan, Meimei Li, J.F. Stubbins, J. Nucl. Mater. 343 (2005) 302.
[35] X. Pan, X. Wu, Meimei Li, J.F. Stubbins, J. Nucl. Mater. 329–333 (2004) 1088.
[36] M.S. Wechsler, in: The Interaction of Radiation with Solids, North-Holland, Amsterdam, 1964.
[37] R.L. Fish, J.L. Straalsund, C.W. Hunter, J.J. Holmes, ASTM Spec. Tech. Publ. vol. 529, 1973, p. 149.
[38] H.S. Rosenbaum, G.F. Rieger, D. Lee, Metall. Trans. 5 (1974) 1867.
[39] M. Eldrup, B.N. Singh, J. Nucl. Mater. 251 (1997) 132.
[40] M. Eldrup, B.N. Singh, J. Nucl. Mater. 276 (2000) 269.
[41] J.V. Olsen, P. Kirkegaard, N.J. Pedersen, M. Eldrup, in: Proceedings of the14th Int. Conf. Positron Annihilation (Hamilton, Canada 2006), in press.
[42] Meimei Li, N. Hashimoto, T.S. Byun, L.L. Snead, S.J. Zinkle, J. Nucl. Mater. 367–370 (2007) 817.
[43] K. Niebel, M. Wilkens, Phys. Stat. Sol. (a) 24 (1974) 591.
[44] G.V. Műller, PhD thesis, Lausanne, EPFL, 1997.
[45] R.C. Rau, F.S. D'Aragona, R.L. Ladd, Phil. Mag. 21 (1970) 441.
[46] D.M. Maher, B.L. Eyre, Phil. Mag. 23 (1971) 409.
[47] B.L. Eyre, D.M. Maher, A.F. Bartlett, Phil. Mag. 23 (1971) 439.
[48] M.E. Downey, B.L. Eyre, Phil. Mag. 11 (1965) 53.
[49] C.A. English, J. Nucl. Mater. 108&109 (1982) 104.
[50] J.L. Brimhall, B. Mastel, Radiat. Eff. 3 (1970) 203.
[51] M. Eldrup, B.N. Singh, S.J. Zinkle, T.S. Byun, K. Farrell, J. Nucl. Mater. 307–311 (2002) 912.
[52] Meimei Li, T.S. Byun, N. Hashimoto, L.L. Snead, S.J. Zinkle, J. Nucl. Mater. 371 (2007) 53.
[53] W. Schilling, P. Ehrhart, et al., in: M.T. Robinson, F.W. YoungJr. (Eds.), Fundamental Aspects of Radiation Damage in Metals, vol. I, CONF-751006-P1, National Tech. Inform. Service, Springfield, VA, 1975, p. 470.
[54] L. Stals, G. Goedeme, J. Nihoul, Defects in Refractory Metals, Mol, Belgium, 1971.
[55] J. Diehl, in: A. Seeger et al. (Eds.), Vacancies and Interstitials in Metals, North-Holland, 1969, p. 739.
[56] A.K. Seeger, in: Second UN Conference on Peaceful Uses of Atomic Energy, vol. 6. United Nations, New York, 1958, p. 250.
[57] S.M. Ohr, Scripta Metall. 2 (1968) 213.
[58] R.J. Dimelfi, D.E. Alexander, L.E. Rehn, J. Nucl. Mater. 252 (1998) 171.
[59] B. Mastel, H.E. Kissinger, J.J. Laider, T.K. Bierlein, J. Appl. Phys. 34 (1963) 3637.
[60] J.L. Brimhall, Trans. AIME 233 (1965) 1737.
[61] D.F. Hasson, Y. Huang, E. Pink, R.J. Arsenault, Metall. Trans. 5 (1974) 371.
[62] M.S. Wechsler, in: The Inhomogeneity of Plastic Deformation, Am. Society for Metals, Metals Park, OH, 1972, p. 19.
[63] A. Luft, Prog. Mater. Sci. 35 (1991) 97.
[64] M. Li, S.J. Zinkle, J. Nucl. Mater. 361 (2007) 192.